SCIENCE CHINA
Earth Sciences

• RESEARCH PAPER •

June 2014 Vol.57 No.6: 1363–1373
doi: 10.1007/s11430-013-4692-4

# Climate sensitivities of two versions of FGOALS model to idealized radiative forcing

CHEN XiaoLong[1,2], ZHOU TianJun[1,3*] & GUO Zhun[3]

[1] *The National Key Laboratory of Numerical Modeling for Atmospheric Sciences and Geophysical Fluid Dynamics, Institute of Atmospheric Physics, Chinese Academy of Sciences, Beijing 100029, China;*
[2] *College of Earth Science, University of Chinese Academy of Sciences, Beijing 100049, China;*
[3] *Climate Change Research Center, Chinese Academy of Sciences, Beijing 100029, China*

Received December 12, 2012; accepted April 25, 2013; published online December 4, 2013

Projections of future climate change by climate system models depend on the sensitivities of models to specified greenhouse gases. To reveal and understand the different climate sensitivities of two versions of LASG/IAP climate system model FGOALS-g2 and FGOALS-s2, we investigate the global mean surface air temperature responses to idealized $CO_2$ forcing by using the output of abruptly quadrupling $CO_2$ experiments. The Gregory-style regression method is used to estimate the "radiative forcing" of quadrupled $CO_2$ and equilibrium sensitivity. The model response is separated into a fast-response stage associated with the $CO_2$ forcing during the first 20 years, and a slow-response stage post the first 20 years. The results show that the radiative forcing of $CO_2$ is overestimated due to the positive water-vapor feedback and underestimated due to the fast cloud processes. The rapid response of water vapor in FGOALS-s2 is responsible for the stronger radiative forcing of $CO_2$. The climate sensitivity, defined as the equilibrium temperature change under doubled $CO_2$ forcing, is about 3.7 K in FGOALS-g2 and 4.5 K in FGOALS-s2. The larger sensitivity of FGOALS-s2 is due mainly to the weaker negative longwave clear-sky feedback and stronger positive shortwave clear-sky feedback at the fast-response stage, because of the more rapid response of water vapor increase and sea-ice decrease in FGOALS-s2 than in FGOALS-g2. At the slow-response stage, similar to the fast-response stage, net negative clear-sky feedback is weaker in FGOALS-s2. Nevertheless, the total negative feedback is larger in FGOALS-s2 due to a larger negative shortwave cloud feedback that involves a larger response of total cloud fraction and condensed water path increase. The uncertainties of estimated forcing and net feedback mainly come from the shortwave cloud processes.

**climate sensitivity, climate response, feedbacks, FGOALS, CMIP5**

**Citation:** Chen X L, Zhou T J, Guo Z. 2014. Climate sensitivities of two versions of FGOALS model to idealized radiative forcing. Science China: Earth Sciences, 57: 1363−1373, doi: 10.1007/s11430-013-4692-4

Global climate models are the primary tools used for climate change projections. Model climate sensitivity is a critical issue that determines the model response to specified greenhouse-gas forcing. According to the Intergovernmental Panel on Climate Change (IPCC) Fourth Assessment Report (AR4), large spread of climate sensitivity was distinguished among the involved climate models (Meehl et al., 2007). The uncertainty is a major limitation to the projections of future climate changes.

To facilitate the inter-comparison among different models, climate sensitivity is diagnosed based on specific idealized forcing experiments. In the equilibrium state, equilibrium climate sensitivity (ECS), often briefly termed the "climate sensitivity", is measured with the change of global mean surface air temperature (SAT) in a doubled $CO_2$ experiment

*Corresponding author (email: zhoutj@lasg.iap.ac.cn)

run to equilibrium. In order to get more evident climate change signal, the quadrupled $CO_2$ forcing is often used in such kinds of experiment (Bryan et al., 1982; Gregory et al., 2004). For the problem of efficiency and computing cost of long-term simulation to reach an equilibrium state, in the AR4, the climate sensitivity was estimated using an atmospheric model coupled to a simple non-dynamic oceanic model, usually termed as "mixed-layer" or "slab" ocean, for simulating efficiently to a new equilibrium (Randall et al., 2007). The slab version could give a good estimate of the ECS of the corresponding full-coupled model (Danabasoglu et al., 2009). Nevertheless, the slab-version model is different from the fully coupled model used for climate projections. To overcome the limitation, Gregory et al. (2004) proposed a simple regression method, making it possible to estimate the ECS directly from non-steady-state simulation of a fully coupled model. The method to estimate the equilibrium climate response could be accurate to within 10% compared with the real value in the equilibrium state (Li et al., 2012).

Great efforts have been devoted to the development of climate system models in LASG/IAP. Two versions of FGOALS model (see the Section 1) have been involved in the fifth phase of the Coupled Model Intercomparison Project (CMIP5). However, their climate sensitivities to the increase of $CO_2$ remain unknown. The $\Delta T$, changes of globally averaged SAT relative to pre-industrial control run, in the quadrupled $CO_2$ experiments of the two versions of FGOALS model are compared in Figure 1. It is evident that the $\Delta T$ increases rapidly during the first two decades but slowly afterward. The whole period of SAT response to the specified $CO_2$ forcing can be partitioned into a fast-response stage followed by a slow-response stage. At the fast-response stage, the trends are 3.18 and 2.06 K $(20\ yr)^{-1}$ in FGOALS-s2 and FGOALS-g2 respectively, whereas they are 0.51 and 0.61 K $(50\ yr)^{-1}$ at the slow-response stage. Since the $CO_2$ forcing specified in the atmosphere is identical in the two model versions, the equilibrium state temperature, or the ECS, is determined by the responses and feedback processes at the two stages. To understand the different responses between the two versions of FGOALS model to identical $CO_2$ forcing, this study aims to compare the sensitivity of the two models. The processes that influence model sensitivity are analyzed. We show evidence that stronger positive water vapor and albedo feedbacks mainly contribute to the larger sensitivity of FGOALS-s2 than FGOALS-g2 at the fast-response stage, though stronger negative shortwave cloud feedback can partly diminish the ECS of FGOALS-s2 at the slow-response stage.

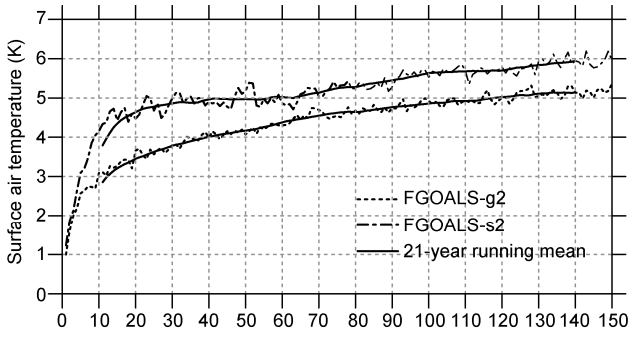


**Figure 1** Time series of 150-yr global mean SAT under quadrupled $CO_2$ scenario relative to piControl run.

## 1 Model and experiment

FGOALS-g2 and FGOALS-s2 are the two versions of the Flexible Global Ocean-Atmosphere-Land System (FGOALS) models developed by LASG/IAP, both of which are involved in CMIP5. The atmospheric component (GAMIL2) of FGOALS-g2 is dispersed by equal-area grid, which is characterized by dense meridional spacing in low latitudes but sparse in high latitudes. The horizontal resolution of GAMIL2 is about 2.8°×3° and vertical direction is σ-coordinate with 26 model levels. The atmospheric component (SAMIL2) of FGOALS-s2 employs a spectral dynamical framework with R42 truncation that is about 2.8°×1.7°, and hybrid vertical coordinate with 26 model levels. GAMIL2 and SAMIL2 are coupled to the same ocean model (LICOM2) with resolutions about 1°×1° in the horizontal and 30 levels in z-coordinate. The ice components in FGOALS-g2 and FGOALS-s2 are CICE4 and CSIM5 respectively (Li et al., 2013; Bao et al., 2013). In FGOALS-g2, the shortwave absorption is estimated by a δ-Eddington approximation method (Briegleb, 1992) and the longwave radiative transfer is based on an absorptivity/emissivity formulation (Ramanathan et al., 1986). A diagnostic Slingo-type scheme (Slingo, 1987) is employed to calculate the cloud fraction that depends on relative humidity, water vapor, atmospheric stability, and convective mass fluxes (Collins et al., 2004). In FGOALS-s2, the cloud is diagnosed by a scheme based on vertical motion and relative humidity (Liu et al., 1997). The radiation is figured out by the modified Edwards-Slingo scheme (Edwards et al., 1996; Sun et al., 1999a, 1999b). For detailed information about these two model versions, the reader is referred to Li et al. (2013) and Bao et al. (2013).

The experiment used in present study is one benchmark sensitivity experiment abrupt4xCO2 in CMIP5 experiment table (Taylor et al., 2012). It is the only experiment to determine climate sensitivity and designed for the regression approach of the Gregory-style analysis (Gregory et al., 2004). The experiment is driven by the so-called quadrupled $CO_2$ scenario. It is initialized from the pre-industrial control run (piControl) and imposed instantaneous quadrupling of $CO_2$ concentration relative to pre-industrial. Then the $CO_2$ concentration is fixed and simulated 150 years (Taylor et al., 2012). The SAT yielded by models is equivalent to the widely used air temperature at 2 m height. The shortwave

and longwave components of radiation can be obtained separately. Furthermore, both the all-sky and clear-sky radiation variables at the top of the atmosphere (TOA) are used to distinguish the radiative effects with and without cloud (Ramanathan et al., 1989). The positive direction of radiation is downward in this study. Some basic physical elements are analyzed to understand the different responses and feedbacks in the two versions of FGOALS model, including the vertical profiles of temperature and specific humidity, sea ice concentration, cloud fraction, and liquid water path etc. The whole simulation period (150 years) is used for analysis.

## 2 Method of measuring the ECS

The ECS is defined as the equilibrium change in the SAT after doubling the atmospheric $CO_2$ concentration relative to pre-industry (Randall et al., 2007). Following Gregory et al. (2008), the "forcing" here is defined as the imbalance of radiation at the TOA caused by forcing agent (i.e., the quadrupled $CO_2$ concentration here) before any climate response emerges. The ECS and forcing are diagnosed directly based on the abrupt4xCO2 experiment following the regression method proposed by Gregory et al. (2004).

To the first-order approximation, the relation between the forcing, feedback and response can be expressed as

$$N = F + \alpha\Delta T, \tag{1}$$

where $N$ is the instantaneous radiative imbalance at the TOA, $F$ is the radiative forcing caused by forcing agent, $\alpha$ is the feedback parameter that is the inverse of the climate sensitivity parameter, and $\Delta T$ is the response of SAT relative to original equilibrium climate state (e.g., the piControl run).

With the assumption that $F$ and $\alpha$ are constant, a linear fit of $\Delta T$ against $N$ can derive the value of $F$, which is the intercept at the $N$-axis (without any response in temperature, $\Delta T$=0), and equilibrium temperature $\Delta T_{\mathrm{eqm}}$, which is the intercept at the $\Delta T$-axis (fully responding and reaching a new balance, $N$=0). The value for $\alpha$ is estimated from the slope of the fitted line.

In fact, the climate response is nonlinear and $\alpha$ is not exactly a constant (Boer et al., 2003). The $F$ and $\Delta T_{\mathrm{eqm}}$ should be estimated separately. For the forcing $F$ estimated by the regression depends on the number of years, Hansen et al. (2005) suggested that 10–30 years run lengths should be used. In this study, we use the first 20-year run to estimate the forcing $F$ and the rest data to estimate the equilibrium temperature response $\Delta T_{\mathrm{eqm}}$. Based on the different temperature response stage shown in Figure 1, this time separation is reasonable. The ECS is simply obtained by dividing the estimated $\Delta T_{\mathrm{eqm}}$ by two, assuming that the climate sensitivity is proportional to the logarithm of $CO_2$ concentration (Manabe et al., 1985; Andrews et al., 2012).

Although we get the forcing at the limit $\Delta T$=0, the forcing has involved several rapid feedbacks, e.g., stratospheric adjustment, cloud, water vapor, lapse rate and land processes etc, since the estimation of forcing is made with the response (Gregory et al., 2004, 2008; Hansen et al., 2005). As proposed by Gregory et al. (2008), to clearly show the effects of different feedbacks, the radiation at the TOA is decomposed into clear-sky longwave (LN), clear-sky shortwave (SN), cloud longwave (LC), and cloud shortwave (SC) fluxes. The LN/SN is yielded directly by model whereas the LC/SC is derived from the difference between clear-sky and all-sky longwave/shortwave radiation. Then we examine the forcing and feedback related to each component.

The geographical distributions of SAT response to quadruped $CO_2$ concentration are non-uniform. The response patterns of the two models show that continents are warmer than oceans and high latitude is warmer than low latitude, especially the region near the North Pole (Figure 2). The warming over the Southern Hemisphere and Arctic region in FGOALS-s2 is larger than FGOALS-g2, whereas the northern Atlantic Ocean has the minimum warming and even some kinds of cooling (Figure 2(b)), which is thought to be related to the change of Atlantic Meridional Overturning Circulation (AMOC). The features suggest that the regional response of SAT to greenhouse-gas radiative forcing is affected by locally complicated heat budget mechanisms. Nevertheless, the response of globally averaged SAT is straightforwardly associated with the energy imbalance at the TOA. Therefore, the defined climate sensitivities of different climate models are comparable at global scale.

During the 500-year piControl run, the SAT in FGOALS-s2 is about 0.51 K higher than that in FGOALS-g2 (Figure 3(a)). The temperature has a drift of $-0.03$ K (100 yr)$^{-1}$ in FGOALS-g2 and $-0.04$ K (100 yr)$^{-1}$ in FGOALS-s2 (Figure 3(a)). The net radiation at the TOA is not completely balanced in the two model versions, with a positive downward flux of 3.30 W m$^{-2}$ in FGOALS-g2 and 0.87 W m$^{-2}$ in FGOALS-s2. The drifts of net radiation flux are 0.01 W m$^{-2}$ (100 yr)$^{-1}$ and 0.02 W m$^{-2}$ (100 yr)$^{-1}$ in FGOALS-g2 and FGOALS-s2 (Figure 3(b)). In order to minimize the effect of climate drift, in the following analysis, the result of piControl run is removed from the abrupt4xCO2 experiment.

## 3 Results

In the following analysis, we first compare the radiative forcings of the quadrupled $CO_2$ in two versions of FGOALS model. The contributions of clear-sky/cloud feedbacks at the fast-response stage to the estimated radiative forcings are analyzed. Then we estimate the ECSs of two model versions. The feedback processes at the fast and slow-response

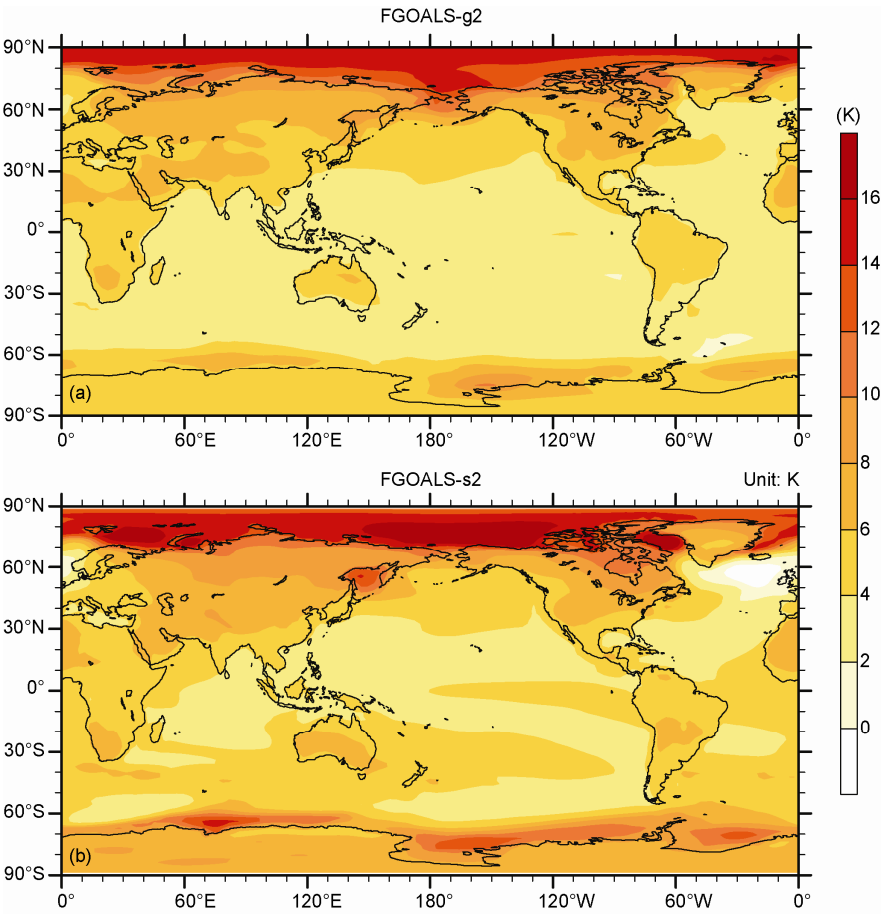


**Figure 2** Geographical distribution of SAT responses to quadrupled $CO_2$ concentration, averaged in 150 simulation years relative to piControl run. (a) FGOALS-g2; (b) FGOALS-s2.

stages are compared.

### 3.1 Forcing and involved feedbacks

The Gregory-style analysis is shown in Figure 4. The radiative forcing caused by quadrupled $CO_2$ is estimated with the first 20-year data, namely the fast-response stage, at the intercept of ordinate axis. The doubled $CO_2$ forcing is 3.64± 0.15 W m$^{-2}$ (the half of quadrupled $CO_2$ forcing in Table 1) in FGOALS-g2 and 3.90±0.20 W m$^{-2}$ in FGOALS-s2. The uncertainty is represented by ±1 standard deviation. The estimation is close to the theoretical value 3.71 W m$^{-2}$ of the doubled $CO_2$ forcing (Myhre et al., 1998; Forster et al., 2006) and the value of 3.74±0.08 W m$^{-2}$ given by Gregory et al. (2004). The difference of the forcing between the two versions of FGOALS model is much less than the spread among CMIP3 models (Gregory et al., 2008) and other CMIP5 models (Andrews et al., 2012).

In order to reveal the respective effect of shortwave/longwave and clear-sky/cloud, the decomposition of the forcing is shown in Figure 5. The forcing components of LN, SN, LC, and SC are the intercepts at ordinate axis of respective TOA radiative components against the $\Delta T$. Due to the infrared protecting of $CO_2$, the longwave clear-sky forcing $F_{LN}$ dominates the total forcing $F$ in two model versions, which are consistent with the results derived from CMIP3 models (Gregory et al., 2008) and other CMIP5 models (Andrews et al., 2012). However, the $F_{LN}$ in FGOALS-s2 is evidently larger than that in FGOALS-g2 (Figure 5, Table 1). Although the difference of $F_{LN}$ may be due partly to the different radiative schemes employed in two AGCMs , i.e., a modified Edwards-Slingo scheme (Sun et al., 1999a) is used in AGCM component of FGOALS-s2, while Ramanathan-Downey scheme (Ramanathan et al., 1986) is used in AGCM component of FGOALS-g2, based on the regression method, the longwave clear-sky feedback $\alpha_{LN}$ is involved in the estimation of $F_{LN}$. We also find that the larger $F_{LN}$ in FGOALS-s2 corresponds to a weaker negative $\alpha_{LN}$ and vice versa in FGOALS-g2 (Table 1), indicating that the process related to $\alpha_{LN}$ should contribute to the $F_{LN}$ differently in FGOALS-g2 and FGOALS-s2.

The $\alpha_{LN}$ is the strongest negative feedback (Figure 5), which includes the negative black-body and lapse-rate feedback, and the positive water vapor feedbacks (Colman, 2003). The water vapor in troposphere can amplify the $CO_2$-induced warming by enhanced greenhouse effect. In

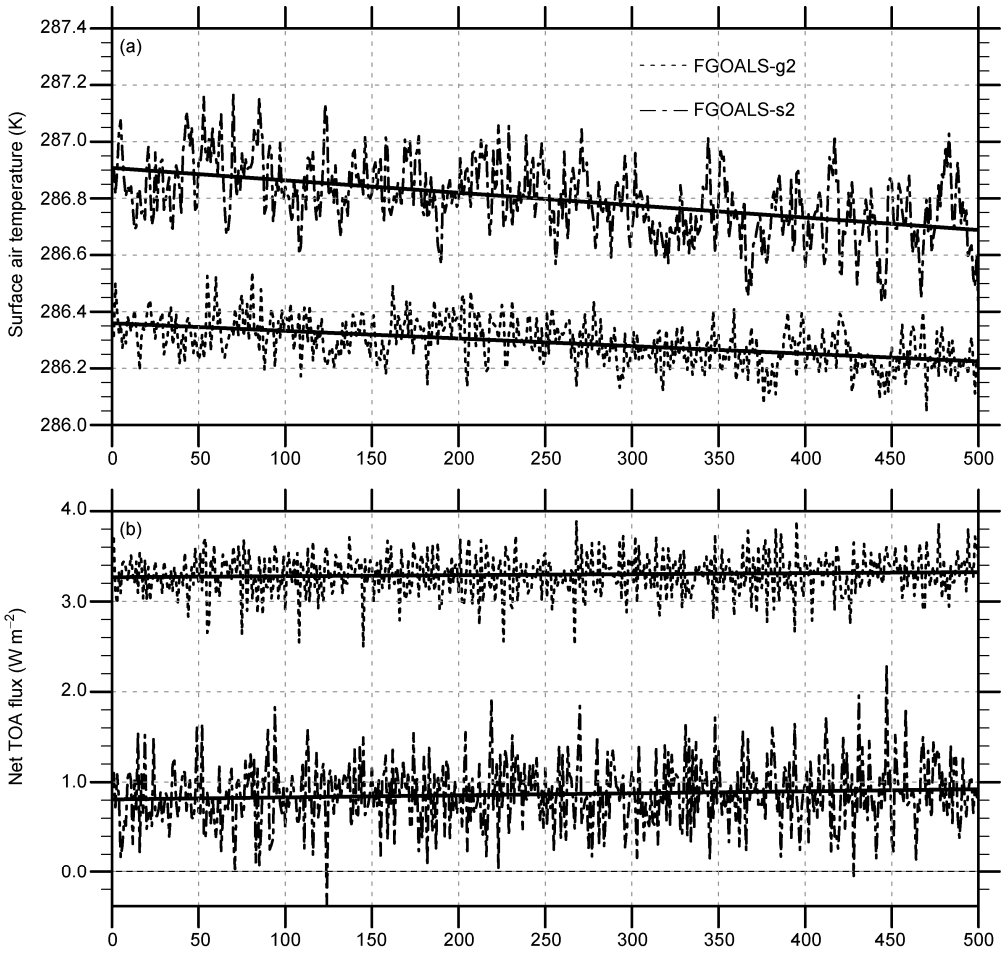


**Figure 3** Globally averaged SAT (a) and net radiation at the TOA of 500-year piControl runand corresponding trends (black bold line) (b).

contrast, the black-body feedback always cools the climate system following the Stefan-Boltzmann law that warmer atmosphere and surface emit more radiation, and the lapse rate feedback is caused by larger upper tropical troposphere warming, which induces more outgoing longwave (Hansen et al., 1981). In order to understand the differences of $F_{LN}$ in two model versions, the $F_{LN}$ is decomposed into the surface longwave (LS) component $F_{LS}$ and clear-sky atmospheric longwave (LA) component $F_{LA}$, as shown in Figure 6. The radiation of clear-sky atmospheric longwave is derived from the TOA clear-sky longwave by subtracting the surface infrared emission, representing the capability of trapping longwave radiation by greenhouse gases in the atmosphere. It shows that the $F_{LA}$, including the $CO_2$ forcing and the related water vapor-lapse rate feedback, is nearly the same as $F_{LN}$, while the $F_{LS}$ is negligible compared with the former (Figure 7(a), Table 1). The water vapor is the most important greenhouse gas and can induce the strongest positive feedback in a warming climate (Colman, 2003). Such a positive water vapor feedback increases the greenhouse gas forcing, given the increased $CO_2$ concentration (Held et al., 2000). The lapse rate feedback can partly offset the effect of water vapor, but the total $\alpha_{LA}$ is still positive in two model versions (Figure 6).

To further demonstrate and compare the positive water-vapor feedback in these two model versions, we examine the difference of the vertical profile of the temperature and specific humidity between FGOALS-s2 and FGOALS-g2 (Figure 8). In FGOALS-s2, the most significantly warm anomalies range from 300 to 700 hPa in the troposphere (Figure 8(a)). It reflects the impact of water vapor and moist adiabatic process. Since the concentration of water vapor in the lower troposphere is larger than that in the upper, once an upward motion anomaly appears, the middle-upper troposphere where the vapor condenses would have stronger temperature anomalies than that in the lower part when the climate condition changes, e.g., under quadrupled $CO_2$ scenario. At the same time, the warmer condition enlarges the saturation water vapor pressure and then the capacity of holding water vapor. Therefore, the water vapor response is more significant in FGOASL-s2, as the specified humidity anomalies shown in Figure 8(b).

The enhanced warming in FGOALS-s2 is evidently larger than that in FGOALS-g2 during the first 20 years (Figure 8(a)). Also, the response of water vapor below 500 hPa is larger in FGOALS-s2 (Figure 8(b)). The stronger response

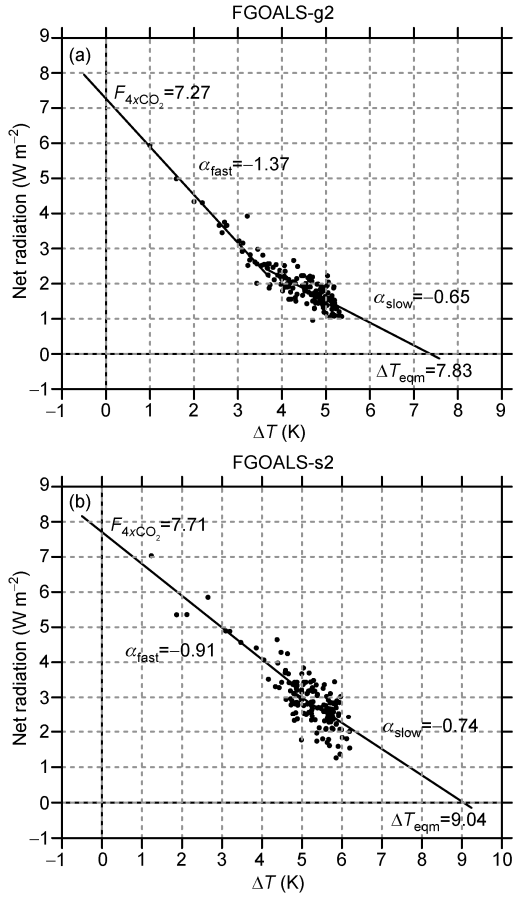


**Figure 4** Net radiation at TOA against the global mean SAT changes under the quadrupled $CO_2$ scenario relative to piControl run. (a) FGOALS-g2; (b) FGOALS-s2. The forcing $F_{4xCO_2}$ is estimated with the fitting at the fast-response stage (the first 20 years), and the equilibrium temperature response $\Delta T_{eqm}$ is estimated at the slow-response stage (the other 130 years). The forcing $F_{4xCO_2}$ (the intercept of ordinate axis), equilibrium temperature $\Delta T_{eqm}$ (the intercept of abscissa axis), and feedback parameters αfast and $\alpha_{slow}$ (the slopes of fitting lines) are labeled.

of water vapor to the $CO_2$ forcing at the fast-response stage in FGOALS-s2 absorbs more longwave in the atmosphere and contributes to the larger $F_{LA}$ and $F_{LN}$. A different situation is seen in FGOALS-g2.

The forcings of $F_{LC}$ and $F_{SC}$, which are related with the cloud properties and much less than $F_{LN}$, also contribute to the net forcing $F$ by offsetting the positive value of $F_{LN}$, especially in FGOALS-s2 (Figure 7(a)). The $F_{LC}$ is negative in both model versions (Figure 5). It indicates that cloud response to $CO_2$ forcing induces the increase of outgoing longwave that reduces the positive forcing enhanced by water vapor. In FGOALS-s2, the $F_{SC}$ plays a similar role by increasing the reflected shortwave, whereas it can be negligible in FGOALS-g2 (Figure 7(a)). The large uncertainty of $F_{SC}$ contributes to most of uncertainty of the estimated net forcing $F$ (Table 1).

Both model versions show that the $F_{SN}$, related with the clear-sky shortwave feedback $\alpha_{SN}$, is small in the net $F$ (Figure 7(a)). It indicates that the process of clear-sky shortwave associated with the change of snow-ice albedo at high latitudes is purely a response to $CO_2$ forcing and its contribution to the net forcing F is small at the fast-response stage.

**Table 1** Estimated $CO_2$ radiative forcing, feedback parameter, equilibrium temperature and the components of longwave/shortwave and clear-sky/cloud in FGOALS-g2 and FGOALS-s2 under quadrupled $CO_2$ scenario derived from the Gregory-style regression[a)]

| | | FGOALS-g2 | FGOALS-s2 |
|---|---|---|---|
| Radiative Forcing (W m$^{-2}$) | $F_{LN}$ | 8.13±0.08 | 10.01±0.12 |
| | $F_{SN}$ | −0.17±0.06 | −0.06±0.11 |
| | $F_{LC}$ | −0.78±0.12 | −1.23±0.15 |
| | $F_{SC}$ | 0.09±0.21 | −1.01±0.52 |
| | $F_{NET}$ | 7.27±0.30 | 7.71±0.41 |
| | $F_{LS}$ | 0.54±0.09 | 0.13±0.10 |
| | $F_{LA}$ | 7.59±0.12 | 9.89±0.14 |
| Feedback parameter (W m$^{-2}$ K$^{-1}$) | $\alpha_{LN}$ | −1.78±0.03 (−1.72±0.02) | −1.37±0.03 (−1.49±0.03) |
| | $\alpha_{SN}$ | 0.70±0.02 (1.05±0.02) | 0.89±0.03 (1.13±0.04) |
| | $\alpha_{LC}$ | 0.07±0.04 (0.18±0.02) | −0.03±0.04 (0.28±0.03) |
| | $\alpha_{SC}$ | −0.36±0.07 (−0.16±0.04) | −0.40±0.13 (−0.66±0.12) |
| | $\alpha_{NET}$ | −1.37±0.10 (−0.65±0.05) | −0.91±0.11 (−0.74±0.09) |
| | $\alpha_{LS}$ | −5.40±0.03 (−5.28±0.02) | −5.20±0.02 (−5.16±0.03) |
| | $\alpha_{LA}$ | 3.62±0.04 (3.56±0.02) | 3.83±0.04 (3.67±0.05) |
| Equilibrium temperature (K) | | 7.4 | 9.0 |

a) The uncertainty is represented by ±1 standard error. For feedback parameter, the value with (without) the parentheses is calculated on the slow (fast)-response stage

### 3.2 ECS and related feedbacks

The equilibrium temperature response $\Delta T_{eqm}$, half of which is used to estimate the ECS, is estimated with the 21-150 years data at the slow-response stage (Figure 4). The ECS is about 3.7 K in FGOALS-g2 and 4.5 K in FGOALS-s2. The $\Delta T_{eqm}$ is determined by the magnitudes of the feedbacks $\alpha_{fast}$ at the fast-response stage and $\alpha_{slow}$ at the slow-response stage. The subscripts "fast" and "slow" of $\alpha$ are used to distinguish the different stages. Stronger negative $\alpha_{fast}$ and $\alpha_{slow}$ (larger their absolute values) result in less climate sensitivity. According to the regression plot (Figure 4), the magnitude of forcing at $\Delta T$=0 could affect the value of $\Delta T_{eqm}$. A larger forcing favors a larger $\Delta T_{eqm}$. However, the difference of estimated forcings $F$ is also the result of different feedbacks. Hence, only the effect of feedbacks on the ECS is studied.

As shown in Figure 4 and Table 1, the difference of $\alpha_{fast}$ is about 0.5 W m$^{-2}$ K$^{-1}$ between FGOALS-s2 and FGOALS-g2, which is five times of that of $\alpha_{slow}$ (about −0.1 W m$^{-2}$ K$^{-1}$), and thus amplifies the sensitivity of FGOALS-s2. Furthermore, Figure 4 shows that after the fast-response

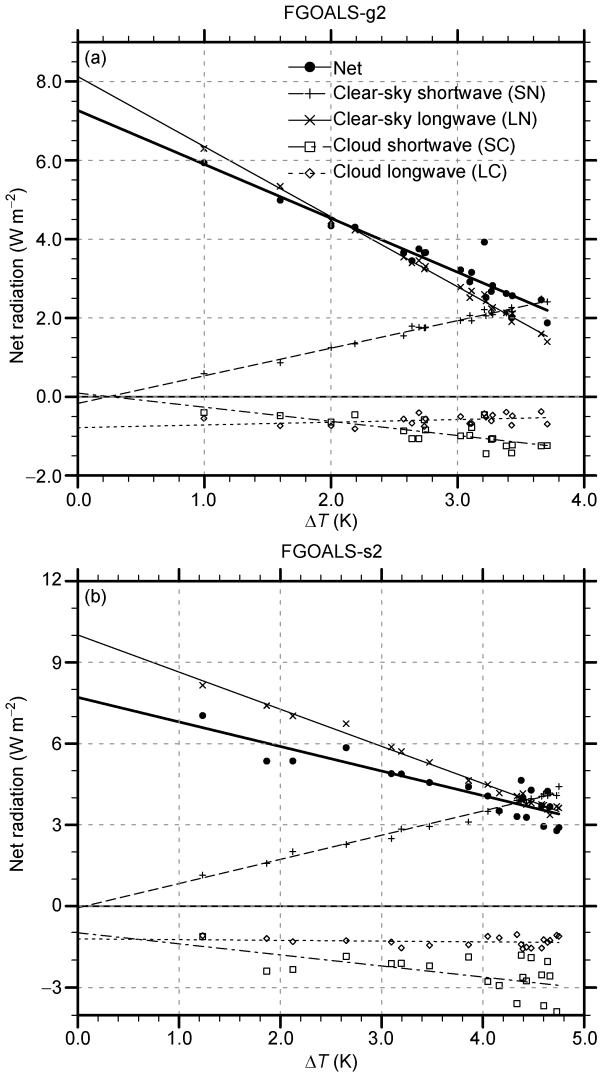


**Figure 5** The decomposition of net forcing at the TOA and feedback at the fast-response stage (the first 20 years) into four components: clear-sky longwave (LN), clear-sky shortwave (SN), cloud longwave (LC), and cloud shortwave (SC). (a) FGOALS-g2; (b) FGOALS-s2.

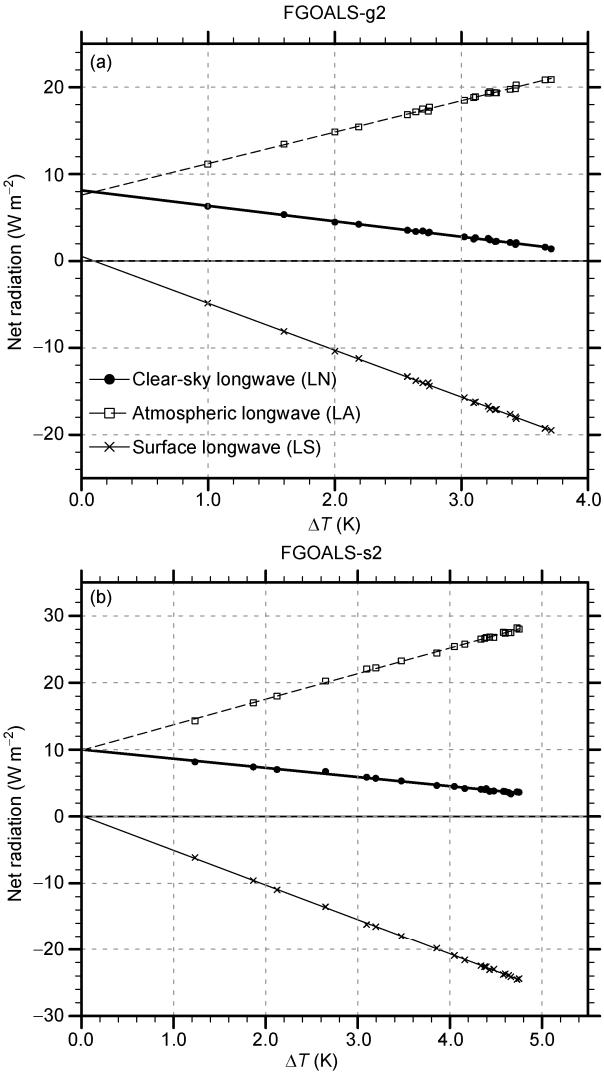


**Figure 6** Same as Figure 5, except for the decomposition of TOA clear-sky longwave (LN) into two components: surface longwave (LS) and atmospheric longwave (LA).

stage the imbalanced radiation at the TOA (*N*-axis) is about 2.2 W m$^{-2}$ in FGOALS-g2 but remains to be 3.4 W m$^{-2}$ in FGOALS-s2. The difference of *N* (about 1.2 W m$^{-2}$) is much larger than that of the estimated forcing *F* (about 0.4 W m$^{-2}$). Therefore, the weaker negative feedback $\alpha_{\text{fast}}$ in FGOALS-s2 is responsible for the larger equilibrium sensitivity.

In order to understand the contribution of shortwave/longwave, clear-sky/cloud feedbacks, the decomposed results of the net feedback $\alpha_{\text{fast}}$ and $\alpha_{\text{slow}}$ are shown in Figure 7(b). For the fast-response stage, it is evident that the differences of $\alpha_{\text{LN}}$ (about 0.4 W m$^{-2}$ K$^{-1}$) and $\alpha_{\text{SN}}$ (about 0.2 W m$^{-2}$ K$^{-1}$) dominate the difference of net $\alpha_{\text{fast}}$ (about 0.5 W m$^{-2}$ K$^{-1}$) between FGOALS-s2 and FGOALS-g2. In FGOALS-s2, the negative longwave clear-sky feedback $\alpha_{\text{LN}}$ is weaker, but the positive shortwave clear-sky feedback $\alpha_{\text{SN}}$ is stronger. As mentioned in above subsection, the weaker negative $\alpha_{\text{LN}}$ is related to the stronger positive feedback of water vapor included in $\alpha_{\text{LA}}$ in FGOALS-s2, which accounts for about 50% difference (about 0.2 W m$^{-2}$ K$^{-1}$) of $\alpha_{\text{LN}}$ (Table 1). The rest of 50% is resulted from the less surface black-body feedback $\alpha_{\text{LS}}$, namely the weaker response of the longwave emitted by the earth surface in FGOALS-s2 (Table 1).

The difference of cloud feedback contributes to the remaining part of –0.1 W m$^{-2}$ K$^{-1}$, which is dominated by the longwave cloud feedback $\alpha_{\text{LC}}$ (Figure 7(b)). The $\alpha_{\text{LC}}$ is positive in FGOALS-g2 but slightly negative in FGOALS-s2 with a relative large uncertainty (Table 1), indicating that longwave cloud responses may be complex and different in two model versions. The uncertainty of net feedback $\alpha_{\text{fast}}$ is dominated by the uncertainty of shortwave cloud radiative feedbacks (Table 1), which is similar to that of the forcing.

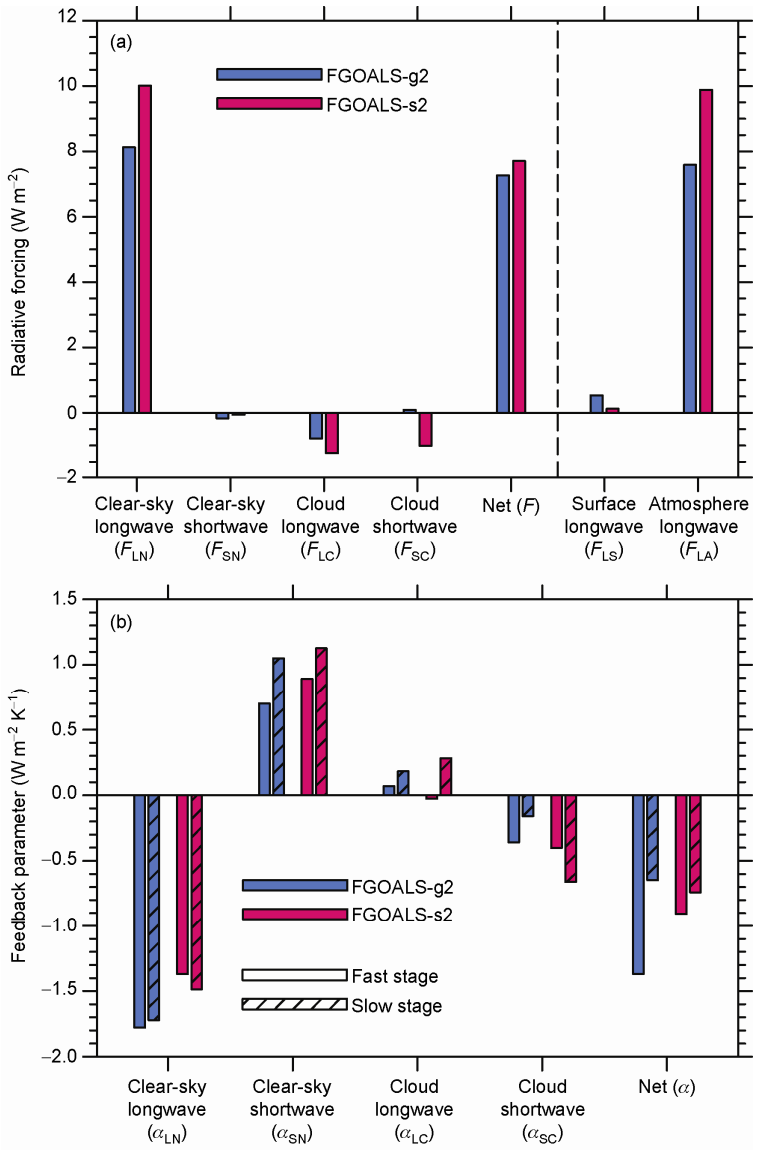


**Figure 7** Comparison of the forcing (a) and feedbacks on the fast and slow-response stage (b) for longwave/shortwave and clear-sky/cloud components in FGOALS-g2 and FGOALS-s2.

The $\alpha_{SN}$ is the strongest positive feedback (Figure 7(b)) and includes the reduction of surface albedo that is attributed mainly to the snow-ice albedo feedback at high latitude (Colman, 2003; Winton, 2006). The response of sea-ice concentration shows a more rapid decrease in FGOALS-s2 than that in FGOALS-g2 during the fast-response stage (Figure 9(a)), which is dominated by the melting of the Arctic sea ice in FGOALS-s2 (Figure 9(b)). Such a situation reflects that the positive albedo feedback is stronger in FGOALS-s2 and contributes to the larger $\alpha_{SN}$ than FGOALS-g2. Therefore, the weaker $\alpha_{fast}$ in FGOALS-s2 mainly results from the stronger positive water vapor and albedo feedbacks, and weaker negative black-body feedback.

At the slow-response stage, the features of $\alpha_{LN}$ and $\alpha_{SN}$ are similar to those at the fast-response stage (Figure 7(b)), except that $\alpha_{SN}$ is evidently stronger and especially in FGOALS-s2, mainly characterized by the sea-ice decrease in the Southern Ocean rather than the Arctic region (Figure 9(c)). The weaker negative $\alpha_{LN}$ and stronger positive $\alpha_{SN}$ contributes to a weaker negative feedback of FGOALS-s2. However, the net negative feedback $\alpha_{slow}$ is slightly stronger in FGOALS-s2 than FGOALS-g2. This tends to reduce the equilibrium sensitivity of FGOALS-s2 (Figure 4). In contrast to the fast-response stage, the negative $\alpha_{SC}$ in FGOALS-s2 is about –0.5 W m$^{-2}$ K$^{-1}$ stronger than that in FGOALS-g2 at the slow-response stage, which is the largest difference among the four feedback components (Figure 7(b), Table 1). It suggests that the stronger $\alpha_{slow}$ in FGOALS-s2 is dominated by the stronger $\alpha_{SC}$.

In view of the complexity of cloud feedback, we further examine the evolving response of total cloud fraction and

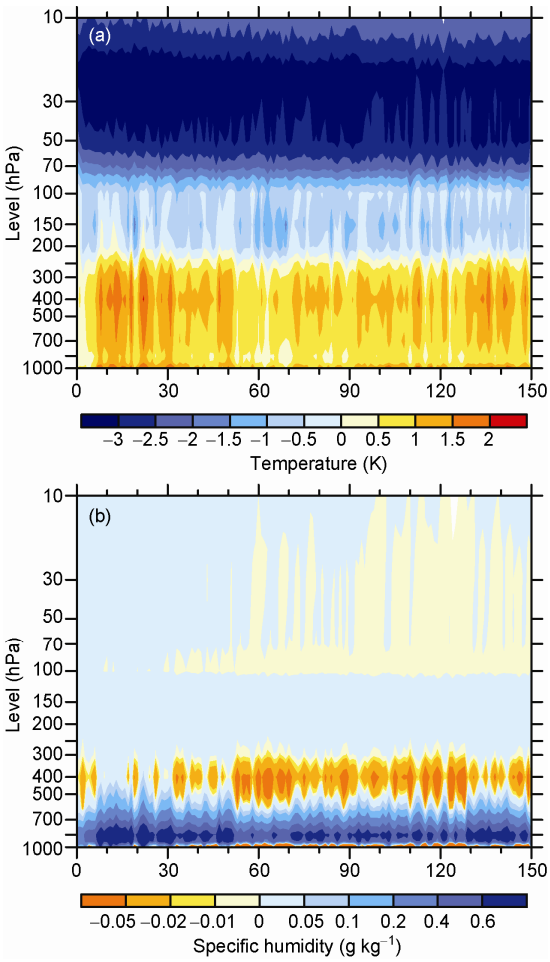


**Figure 8** The difference of response of temperature profile (a) and specific humidity profile (b) between FGOALS-s2 and FGOALS-g2 under the quadrupled $CO_2$ scenario relative to piControl run.

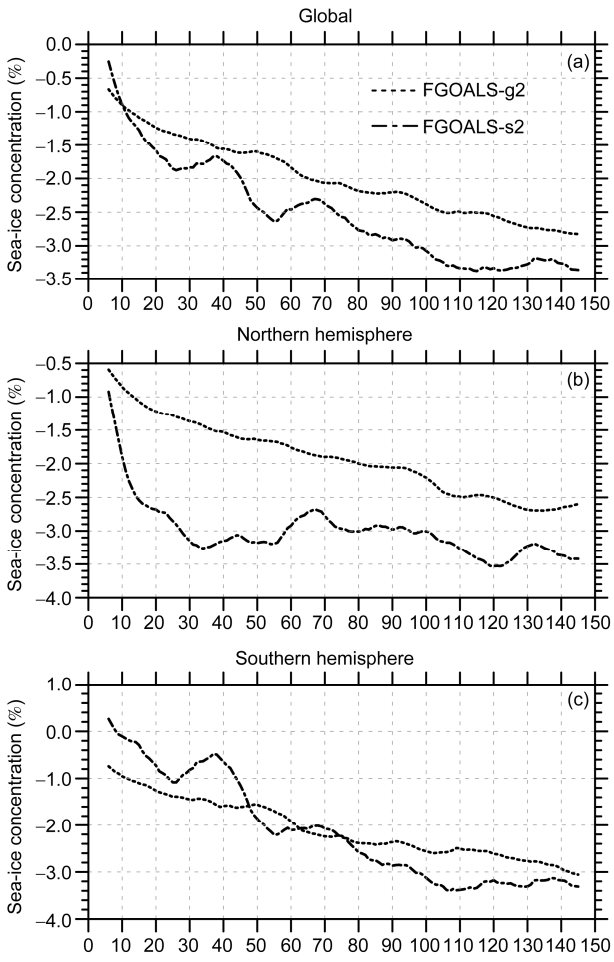


**Figure 9** Global (a), Northern Hemisphere (b) and Southern Hemisphere (c) sea-ice concentration response of 11-year running mean under the quadrupled $CO_2$ scenario relative to piControl run.

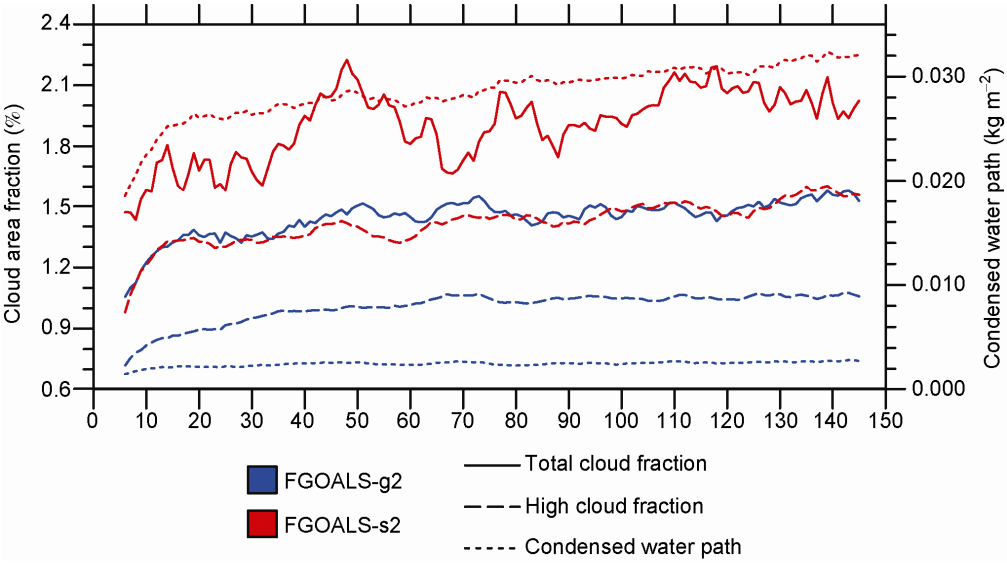


**Figure 10** The response of total cloud fraction (solid line, left *Y*-axis), high cloud fraction (dashed line, left *Y*-axis), and condensed water path (dotted line, right *Y*-axis) under the quadrupled $CO_2$ scenario relative to piControl run.

condensed water path which usually affect the shortwave cloud radiative process (Somerville et al., 1984; Roeckner et al., 1987). As shown in Figure 10, the increasing responses of total cloud fraction and condensed water path to the warming are evidently larger in FGOALS-s2. In particular, the difference is the most evident in the response of condensed water that is extremely weak in FGOALS-g2 resulting in the weaker negative $\alpha_{SC}$ in FGOALS-g2 than that in FGOALS-s2.

In addition, the $\alpha_{LC}$ on the slow-response stage is positive in the two model versions and slightly larger in FGOALS-s2. To understand the difference, the evolution of high cloudiness in these two model versions is also compared in Figure 10. The response of high cloud fraction in FGOALS-s2 is stronger than that in FGOALS-g2, which tends to result in a stronger longwave cloud radiative positive feedback (Figure 7(b)) by absorbing the infrared radiation from lower atmosphere (Wetherald et al., 1988). The stronger condensed water path response in FGOALS-s2 also tends to cause a stronger longwave cloud feedback (Taylor et al., 1992).

In general, compared with FGOALS-g2, although FGOALS-s2 has stronger negative net cloud feedback at the slow-response stage that favors the reduction of climate sensitivity, the stronger positive vapor feedback and albedo feedback, especially at the fast-response stage, overwhelm the negative effect from cloud and finally result in a more sensitive system.

## 4 Summary

To understand why the surface air temperature responses of two versions of IAP/LASG FGOALS model to identical $CO_2$ forcing are different, model climate sensitivities are studied using the benchmark experiments abrupt4xCO2, namely the quadrupled $CO_2$ scenario. The model sensitivity is estimated by using Gregory-style regression method. To better estimate $CO_2$ radiative forcing and ECS, we do regressions in the first 20 years and the rest 130 years separately. These two periods correspond to the fast temperature response and slow response stage respectively. The forcing and feedbacks are decomposed into longwave/shortwave and clear-sky/cloud components to reveal the relative contributions to the different sensitivities. The main conclusions are summarized as follows.

(1) The estimated quadrupled $CO_2$ radiative forcings are 7.27 W m$^{-2}$ in FGOALS-g2 and 7.71 W m$^{-2}$ in FGOALS-s2. The difference of forcing involves the different feedbacks at the fast-response stage, which is dominated by the longwave clear-sky feedback $\alpha_{LN}$. A weaker negative $\alpha_{LN}$ corresponds to a larger estimated forcing. Water vapor feedback is included in $\alpha_{LN}$. A more rapid response of water vapor in FGOALS-s2 is responsible for the weaker $\alpha_{LN}$ and larger estimated forcing. In two model versions, the forcing involving the cloud processes tends to be negative and offset the enhancing effect caused by water vapor. The main uncertainty of estimated forcing comes from the shortwave cloud process.

(2) The estimated ECS is about 3.7 K in FGOALS-g2 and 4.5 K in FGOALS-s2. The larger sensitivity in FGOALS-s2 is dominated by the weaker negative net feedback $\alpha_{fast}$ at the fast-response stage. The weaker negative $\alpha_{fast}$ in FGOALS-s2 is due mainly to the longwave and shortwave clear-sky feedback, which is respectively related to a faster increase of water vapor and decrease of sea ice in FGOALS-s2. The change of sea ice at the fast-response stage in FGOALS-s2 is characterized by a sharp decrease in the Arctic region compared with FGOALS-g2.

At the slow-response stage, the features of clear-sky feedbacks are similar to those at the fast-response stage, which is characterized by less sea ice in the Southern Ocean and more water vapor in FGOALS-s2 than that in FGOALS-g2. However, the net negative feedback $\alpha_{slow}$ is stronger in FGOALS-s2, which tends to reduce its equilibrium sensitivity. The stronger $\alpha_{slow}$ in FGOALS-s2 is resulted from the stronger negative shortwave cloud feedback $\alpha_{SC}$ which is related to the more rapid response of total cloud fraction and condensed water path. The larger positive longwave cloud feedback $\alpha_{LC}$ in FGOALS-s2 is associated with a stronger high-cloud response at the slow-response stage. The shortwave cloud feedback contributes to major uncertainties in the estimated net feedback.

*This study was supported by the National Science Fund for Distinguished Young Scholars (Grant No. 41125017), the "Strategic Priority Research Program — Climate Change: Carbon Budget and Related Issues" of the Chinese Academy of Sciences (Grant No. XDA05110301) and the National Program on Key Basic Research Project of China (Grant No. 2010CB951904).*

Andrews T, Gregory J M, Webb M J, et al. 2012. Forcing, feedbacks and climate sensitivity in CMIP5 coupled atmosphere-ocean climate models. Geophys Res Lett, 38: L09712, doi: 10.1029/2012GL051607

Bao Q, Lin P, Zhou T, et al. 2013. The Flexible Global Ocean-Atmosphere-Land System model, Spectral Version 2: FGOALS-s2. Adv Atmos Sci, 30: 561–576

Boer G J, Yu B. 2003. Climate sensitivity and climate state. Clim Dyn, 21: 167–176

Briegleb B P. 1992. Delta-Eddington approximation for solar radiation in the NCAR Community Climate Model. J Geophys Res, 97: 7603–7612

Bryan K, Komro F G, Manabe S, et al. 1982. Transient climate response to increasing atmospheric carbon dioxide. Science, 215: 56–58

Collins W D, Rasch P J, Boville B A, et al. 2004. Description of the NCAR Community Atmosphere Model (CAM3). Tech Rep NCAR/TN-464+STR, National Center for Atmospheric Research, Boulder, CO

Colman R. 2003. A comparison of climate feedbacks in general circulation models. Clim Dyn, 20: 865–873

Danabasoglu G, Gent P R. 2009. Equilibrium climate sensitivity: Is it accurate to use a slab ocean model? J Clim, 22: 2494–2499

Edwards J M, Slingo A. 1996. Studies with a flexible new radiation code. I: Choosing a configuration for a large-scale model. Q J R Meteorol Soc, 122: 689–719

Forster P M D, Taylor K E. 2006. Climate forcings and climate sensitivities diagnosed from coupled climate model integrations. J Clim, 19: 6181–6194

Gregory J M, Ingram W J, Palmer M A, et al. 2004. A new method for diagnosing radiative forcing and climate sensitivity. Geophys Res Lett, 31: L03205

Gregory J, Webb M. 2008. Tropospheric adjustment induces a cloud component in $CO_2$ forcing. J Clim, 21: 58–71

Hansen J, Johnson D, Lacis A, et al. 1981. Climate impacts of increasing carbon dioxide. Science, 213: 957–966

Hansen J, Sato M, Ruedy R, et al. 2005. Efficacy of climate forcings. J Geophys Res, 110: D18104

Held I M, Soden B J. 2000. Water vapor feedback and global warming. Annu Rev Energy Environ, 25: 441–475

Li L J, Lin P, Yu Y, et al. 2013. The Flexible Global Ocean-Atmosphere-Land System model: Grid-point Version 2: FGOALS-g2. Adv Atmos Sci, 30: 543–560

Li C, von Storch J S, Marotzke J. 2012. Deep-ocean heat uptake and equilibrium climate response. Clim Dyn, 40: 1071–1086

Liu H, Wu G X. 1997. Impacts of land surface on climate of July and onset of summer monsoon: A study with an AGCM plus SSiB. Adv Atmos Sci, 14: 289–308

Manabe S, Bryan K. 1985. $CO_2$-induced change in a coupled ocean-atmosphere model and its paleoclimatic implications. J Geophys Res, 90: 11689–11707

Meehl G A, Stocker T F, Collins W D, et al. 2007. Global climate projections. In: Solomon S, et al., eds. Climate Change 2007: The Physical Science Basis. Contribution of Working Group I to the Fourth Assessment Report of the Intergovernmental Panel on Climate Changes. Cambridge University Press. 747–845

Myhre G, Highwood E J, Shine K P, et al. 1998. New estimates of radiative forcing due to well mixed greenhouse gases. Geophys Res Lett, 25: 2715–2718

Ramanathan V, Cess R D, Harrison E F, et al. 1989. Cloud-radiative forcing and climate: Results from the Earth Radiation Budget Experiment. Science, 243: 57–63

Ramanathan V, Downey P. 1986. A nonisothermal emissivity and absorptivity formulation for water vapor. J Geophys Res, 91: 8649–8666

Randall D A, Wood R A, Bony S, et al. 2007. Climate models and their evaluation. In: Solomon S, et al., eds. Climate Change 2007: The Physical Science Basis. Contribution of Working Group I to the Fourth Assessment Report of the Intergovernmental Panel on Climate Changes. Cambridge University Press. 589–662

Roeckner E, Schlese U, Biercamp J, et al. 1987. Cloud optical depth feedbacks and climate modeling. Nature, 329: 139–140

Slingo J M. 1987. The development and verification of a cloud prediction scheme for the ECMWF model. Q J R Meteorol Soc, 113: 899–927

Somerville R C J, Remer L A. 1984. Cloud optical thickness feedbacks in the $CO_2$ climate problem. J Geophys Res, 89: 9668–9672

Sun Z A, Rikus L. 1999a. Improved application of exponential sum fitting transmissions to inhomogeneous atmosphere. J Geophys Res, 104: 6291–6303

Sun Z A, Rikus L. 1999b. Parametrization of effective sizes of cirrus-cloud particles and its verification against observations. Q J R Meteorol Soc, 125: 3037–3055

Taylor K E, Ghan S J. 1992. An analysis of cloud liquid water feedback and global climate sensitivity in a general circulation model. J Clim, 5: 907–919

Taylor K E, Stouffer R J, Meehl G A. 2012. An overview of CMIP5 and the experiment design. Bull Am Meteorol Soc, 93: 485–498

Wetherald R T, Manabe S. 1988. Cloud feedback processes in general circulation models. J Atmos Sci, 45: 1397–1415

Winton M. 2006. Surface albedo feedback estimates for the AR4 climate models. J Clim, 19: 359–365